

Insight into the Effect of Iodine Doping Soft Carbon and Iodine Functional Separator for Lithium-Sulfur Batteries

Yan Zhang,^[a, b] Shubhadeep Pal,^[b] Yujie Yang,^[a] Cong Huang,^[a] Jiande Wang,^[b] Petru Apostol,^[b] Zheng Liu,^[c] Aiping Hu,^[a] Alexandru Vlad,^[b] and Xiaohua Chen^{*[a]}

Doping carbonaceous materials are regarded as prospective cathode candidates for high-performance lithium-sulfur (Li–S) batteries. In this study, we construct a dual functional modification system, including iodine-doped soft carbon (I-SC) and iodine functional separator for Li–S batteries. The formation of C–I bonds in the carbon skeleton increases the carbon interlayer spacing and displays a powerful chemical adsorption ability and electrocatalytic activity for polysulfide conversion. In addition, semi-hollow micro-rods-structure soft carbon not only

accommodates the volume expansion of sulfur, but also provides a continuous conductive network to transport Li^+ and electrons over cycling. Furthermore, by assisting with poly-iodide (e.g., I_3^- and I_5^-) modified separator, the polysulfide migration can be further controlled, resulting in a high capacity of 956 mAh g^{-1} at 0.2 C after 300 cycles. This work represents the importance of I-doping and provides the potential of soft carbon for low-cost and scalable fabrication of energy storage systems.

Introduction

The growing demands for energy system have inspired intense efforts toward the development of various rechargeable batteries to replace the current lithium-ion batteries (LIBs).^[1] Lithium-sulfur (Li–S) batteries are very promising candidates due to the high specific energy (2600 Wh kg^{-1}), theoretical specific capacity (1675 mAh g^{-1}), and abundant sulfur resources.^[2,3] However, Li–S batteries are plagued by multiple obstacles, such as poor reaction kinetics and the shuttle effect of discharge intermediates.^[4] To date, decorating nonpolar carbon materials with polar groups and heteroatoms has been proven as an essential technique to promote the adsorption capability and the redox kinetics of lithium polysulfides (LiPSs).^[5] Whereas, polar materials, such as metal oxides,^[6] metal sulfides,^[7] metal nitrides,^[8] and metal-organic frameworks,^[9] are difficult to realize the practical commercialization, owing to the high cost of raw materials and complex synthetic routes. Therefore, considering the natural richness of carbon materials and the effectiveness of heteroatoms doping, it is extremely

nontrivial to embrace a reasonable carbon material, and use the one-spot carbonization-doping method to achieve the improvement of Li–S performance for subsequent industrialization.^[10] The degree of graphitization of carbon materials is closely linked to the electrical conductivity, which is the key factors for the reaction kinetics of LiPSs conversion process. In addition, the general method is to encapsulate sulfur with diverse porous carbon materials, notably mesoporous carbon. As a result, using heteroatoms-doped mesoporous soft carbon as a sulfur supporter maybe helpful to synergistically enhance sulfur content and mitigate the dissolution of LiPSs into electrolytes.

Recently, extensive research has proved that heteroatoms (N, O, P, and S) doping carbon materials as promising sulfur hosts can improve the electrochemical performance of Li–S batteries. N and O are one of the most widely investigated dopants. Carbon materials with N and O, show strong chemisorption for LiPSs, because of the strong Lewis acid-base interaction between Li^+ cation in LiPSs and electro-negative N or O atoms.^[11] For P-doped carbon materials,^[12] P-graphene with increased polarity has stronger chemical anchoring of LiPSs, due to the enhanced electron localization on P-graphene, which is consistent with the fact that P atoms have more valence electrons than C atoms. In addition, S-doped carbons^[13] mainly form strong interactions between the polysulfide anions and doped S atoms (S–S) to enhance the chemisorption of LiPSs. Moreover, the co-doping strategy has been proven to be beneficial to the high-performance of Li–S batteries through synergistic effect or combined actions.^[11f,12d,13a,e,14]

Iodine atoms, with relatively high electronegativity ($\chi = 2.66$ for I, $\chi = 2.55$ for C) and a larger radius of iodine (140 pm), are a potential dopant to optimize the electronic structure and increase *d*-spacing of carbon materials.^[15] In addition, soft carbon with good conducting network, adjust-

[a] Dr. Y. Zhang, Dr. Y. Yang, Dr. C. Huang, Prof. A. Hu, Prof. X. Chen
College of Materials Science and Engineering
Hunan Province Key Laboratory for Advanced Carbon Materials and Applied Technology
Hunan University, Changsha 410082, China
E-mail: xiaohuachen@hnu.edu.cn

[b] Dr. Y. Zhang, Dr. S. Pal, Dr. J. Wang, Dr. P. Apostol, Prof. A. Vlad
Institute of Condensed Matter and Nanosciences
Université catholique de Louvain
Louvain-la-Neuve 1348, Belgium

[c] Dr. Z. Liu
College of Materials and Chemical Engineering
All-Solid-State Energy Storage Materials and Devices Key Laboratory of Hunan Province
Hunan City University, Yiyang, 413000, China

 Supporting information for this article is available on the WWW under <https://doi.org/10.1002/batt.202200124>

able interlayer spacing and multiple chemical reactivity sites, can serve as hosts for sulfur cathodes.^[16] Inspired by the above considerations, the iodine-doped soft carbon material is undoubtedly a promising candidate for high performance and future scale production of Li–S batteries. Considering the restricted active sites and inadequate internal space in cathodes,^[17] the functionalization of separator is an effective and reliable approach to trap LiPSs, particularly in high sulfur loading hosts.^[18] Yibo He^[19] et al. fabricated a “polysulfide-phobic” surface into a separator to restrain the shuttle effect and perform a superior cycling stability of Li–S batteries. In short, it is necessary to simultaneously functionalize the sulfur hosts and the separator to greatly restrain the “shuttle effect” and further improve the stability of Li–S batteries.

In this work, we designed an iodine-doped soft carbon and iodine-modified separator to explore the effect of iodine on Li–S batteries. We’re attributing that to a few factors. First, the unique semi-hollow micro-rods structure of iodine-doped soft carbon, which consists of plentiful nano-sheets and cavities, is favorable to store relatively high load of sulfur and infiltrate electrolytes in the internal structure. Second, I atoms in I-SC have a larger radius and higher electronegativity value than that of C, which can facilitate the diffusion of Li-ions and effectively adsorb negatively polysulfide owing to the increased carbon spacing and the positively polarized carbon structure, respectively. Third, based on theoretical calculations, the decomposition barrier of Li_2S on I-SC is much smaller than that of SC, and the electrocatalytic activity of I-SC would accelerate LiPSs into shorter chains. Finally, to further optimize the overall design, we have used the I-modified separator to suppress the diffusion of LiPSs by constructing a “polysulfide-phobic” surface, but Li^+ ions are allowed to pass through the electrolytes by electrostatic attraction.

Results and Discussion

As shown in Figures 1(a and b) and S1, the I-SC/S, I-SC and SC exhibit a unique semi-hollow micro-rods structure with abundant nanosheets and cavities, which can accommodate sulfur species in its void space and buffer the volume expansion during the continual charging/discharging process. The crystal structure of SC, I-SC and I-SC/S was examined by XRD and the corresponding results are shown in Figure 1(c). Compared to SC, the (002) diffraction peak of I-SC located at 21.6° shifts to a smaller angle, which means that the carbon interlayer distance increases from 3.5 to 4.1 Å (based on Bragg’s law) because of the introduction of I atom. The high-resolution TEM image (Figure S1) also shows the disordered lattice fringes (~0.40 nm of I-SC and ~0.35 nm of SC). In addition, XRD patterns of I-SC/S from 10° to 80° are in accordance with the orthorhombic sulfur phase (PDF# 08-0247), indicating successful sulfur loading. Meanwhile, Raman spectroscopy was collected to explore the carbon structure. Figure 1(d) shows a little downshift of the peaks at 1340 and 1591 cm⁻¹ in I-SC and I-SC/S, compared to that of SC (1356 and 1607 cm⁻¹), which are generally assigned to the D-band and G-band associated with the sp³-type carbon

and sp² graphite-like structure, respectively.^[20] These variations originate from the different chemical environment of carbon after I-doping. In addition, the intensity ratios of the D-band over the G-band (I_D/I_G) are calculated at 1.16, 1.21 and 1.20, corresponding to SC, I-SC and I-SC/S, respectively. These results indicate that I-doping can change the chemical environment of carbon structure and induce some extrinsic defects. In addition, the peaks of I-SC/S at 154, 218 and 469 cm⁻¹ correspond to the S–S bonds, confirm the presence of sulfur, once again.^[21] Moreover, further certification can be obtained from the FTIR spectra, as shown in Figure 1(e). The peak at 1067 cm⁻¹ is attributed to the stretching vibrations of C–S/C–O bonds and the peaks centered at 471–672 cm⁻¹ are assigned to C–I stretching vibrations, demonstrating the successful sulfuration and I-doping, respectively. Moreover, another three vibration peaks are found, including C–O (1036–1197 cm⁻¹), C–C (1380 cm⁻¹) and C=C (1628 cm⁻¹).^[22]

To investigate the surface compositions and valence states of I-SC and I-SC/S, X-ray photoelectron spectroscopy (XPS) was further performed. Figure 1(f) reveals the presence of C, O, I and S elements. As shown in Figure 1(g), the two representatives I 3d peaks can be observed at 619.4 eV and 630.8 eV, corresponding to the I 3d_{5/2} and I 3d_{3/2}. The I 3d_{5/2} spectrum of I-SC and I-SC/S is fitted to C–I bonds (619.4 eV).^[23] The high-resolution S 2p spectra in Figure 1(h) is deconvoluted into three peaks, and the binding energies located at 164.1, 165.2 and 168.1 eV are attributed to S 2p_{3/2}, S 2p_{1/2} and S–O bonding.^[24] In addition, the energy dispersive X-ray (EDX) mapping of I-SC also shows the homogeneous distribution of I, C, S, and O elements throughout the particles (Figure S2). The pore structure of SC and I-SC were measured by N₂ adsorption/desorption analysis (Figure S3a and b). The type-IV isotherms linked with H3 hysteresis loops symbolize the appearance of mesoporous structure in SC and I-SC. The Brunauer–Emmett–Teller specific surface area of SC is 14 m² g⁻¹, while I-SC is up to 130 m² g⁻¹, suggesting that the iodine decomposition and I-doping process of SC would promote the enlargement of carbon layer and obtain higher specific area. Combined with Figure S3(b), the pore size distribution can be observed in the range of 2–8 nm, which confirms that SC and I-SC samples are rich in mesoporous. Moreover, the sulfur content in I-SC/S was approximately 80 wt% (Figure S3c).

To evaluate the adsorption ability between I-SC and polysulfides, a visual adsorption test was performed by taking Li_2S_6 as the representative LiPSs. As shown in Figure 2(a), in the presence of SC, the fresh yellow Li_2S_6 solution has slightly changes, which is due to the weak physical confinement of SC. While I-SC shows stronger adsorption than SC, suggesting that I-SC has a stronger LiPSs affinity than SC. Furthermore, in UV-vis absorption spectra (Figure 2a), Li_2S_6 solution with I-SC exhibits the lowest absorbance at 263 nm, which also efficiently confirms LiPSs trapping. In addition, XPS data were collected on the recovered solid (‘I-SC– Li_2S_6 ’).^[25] After contact with I-SC, the S 2p spectrum (Figure 2b) reveals the new sulfur environments between 173 and 167 eV, which can be fitted with polythionate complex. The new sulfur species possibly arise from

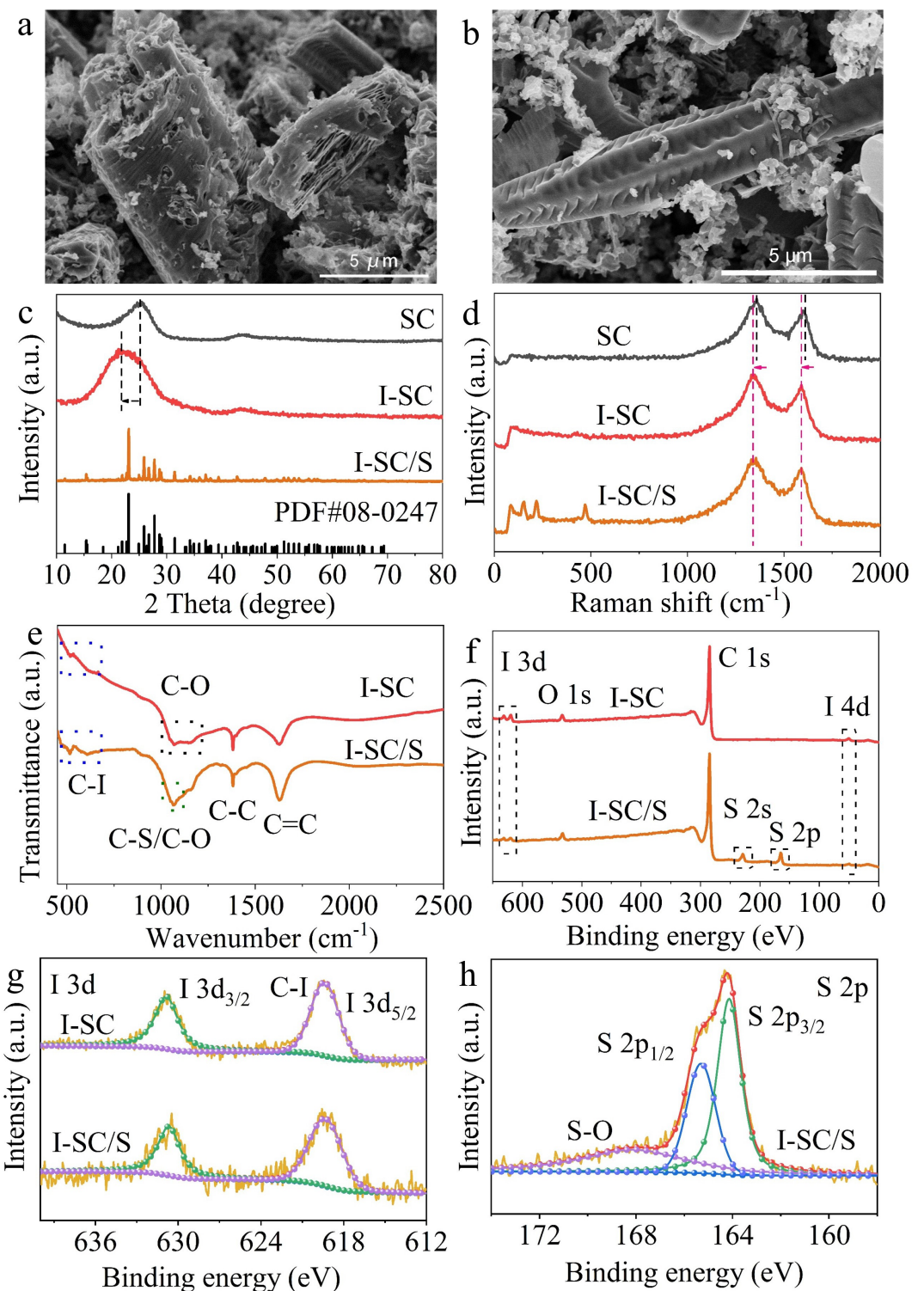


Figure 1. SEM images of a) I-SC, b) SC. c) XRD pattern, d) Raman spectra of SC, I-SC and I-SC/S, e) FTIR spectra. f) XPS spectra and corresponding high-resolution XPS spectra of g) I 3d and h) S 2p.

the surface redox reaction between Li_2S_6 and I-SC. Considering I^- is in its reduced state, we proposed that the generation of polythionate could be from the disproportionation reaction, i.e., $\text{S}_6^{2-} \rightarrow [\text{S}_x(\text{SO}_3)]^{2-} + \text{S}_y^{2-}$ ($0 < x < 6$, $y < 6$) in the presence of I-SC, which can act as the electro-catalyst.^[26]

Based on this formula, the generation of polythionate species could further accelerate the discharge process by converting long-chain LiPSs to short ones. In addition, the I 3d spectra have two peaks at 619.4 eV and 630.8 eV (Figure 2c), which consists with I-SC before adsorption, suggest-

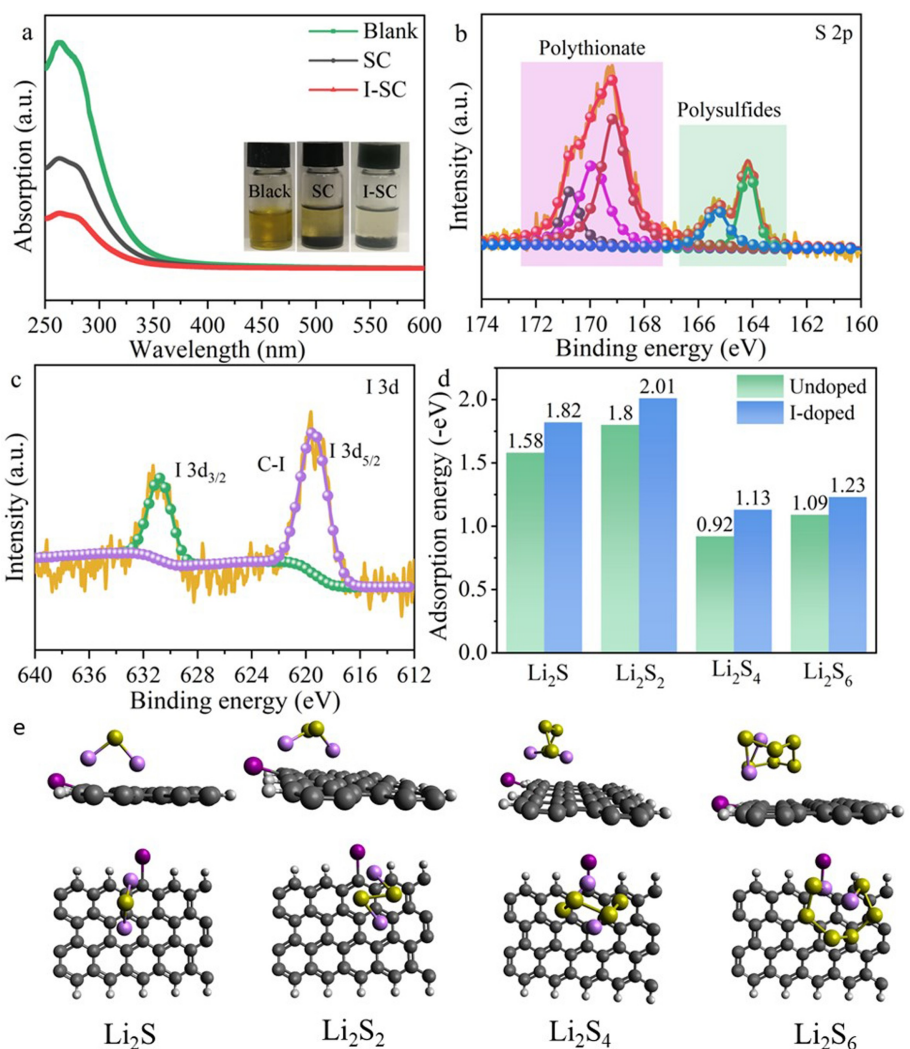


Figure 2. a) UV-vis spectra of Li₂S₆ solution with I-SC, SC, and bare Li₂S₆ solution. Inset photograph corresponds to the optical photograph of above solution. XPS spectrum of b) S 2p and c) I 3d after adsorbed Li₂S₆. d) Theoretical calculated binding energies of Li₂S_x on undoped and I-doped carbon ($x=1, 2, 4, 6$). e) The side views of the most stable configurations of Li₂S_x adsorbed on I-doped carbon.

ing I-C bonds are stable even interacting with the Li₂S₆. The trapping of Li₂S_x ($x=1, 2, 4, 6$) on undoped and I-doped carbon are evaluated by the calculation of the adsorption energy (E_a),^[27]

$$E_a = E_{\text{Li}_2\text{S}_x-\text{Substrate}} - E_{\text{Li}_2\text{S}_x} - E_{\text{Substrate}}$$

where $E_{\text{Li}_2\text{S}_x-\text{Substrate}}$ and $E_{\text{Substrate}}$ are the total energy of the adsorption systems and adsorption substrates, respectively. The calculated adsorption energy is shown in Figure 2(d and e). The adsorption energy of Li₂S_x adsorbed on I-doped carbon are 1.82 eV, 2.01 eV, 1.13 eV and 1.23 eV as x increases from 1 to 6. For undoped carbon, the adsorption energy is 1.58 eV, 1.8 eV, 0.92 eV and 1.09 eV. More negative adsorption energy reveals a stronger adsorption interaction between the I-doped carbon and Li₂S_x molecule. Above all, considering the high electronegativity of I than that of C ($\chi=2.66$ for I and $\chi=2.55$ for C), the strong adsorption of I-SC is mainly attributed to the I-

induced charged carbon plane, through an electrostatic interaction with S_x²⁻ ($1 \leq x \leq 6$).

The symmetrical batteries are assembled by sandwiching separator between two same electrodes filled with Li₂S₆ solution as an electrolyte, which is studied by many researchers to analyze the redox kinetics of polysulfides.^[28] The CV curves were measured at a voltage range from -1.5 to 1.5 V with a scanning rate of 20 mVs⁻¹ (Figure 3a). The I-SC shows a higher current response than that of pristine SC, implying the dynamically enhanced redox kinetics by I-doping. In this case, the CV profile of I-SC at different scan rates was also carried out to further illuminate the catalytic effect. Surprisingly, it remains clearly broad reduction and oxidation peaks even at a fast scan rate of 500 mVs⁻¹, indicating the ultrafast catalytic redox reactions of soluble LiPSs (Figure 3b). In addition, a small semicircle diameter in the Nyquist plot (Figure S4) confirms again that I-SC has a lower resistance of charge transfer, which is associated with valuable I-doping, good electron pathways of I-SC. We also

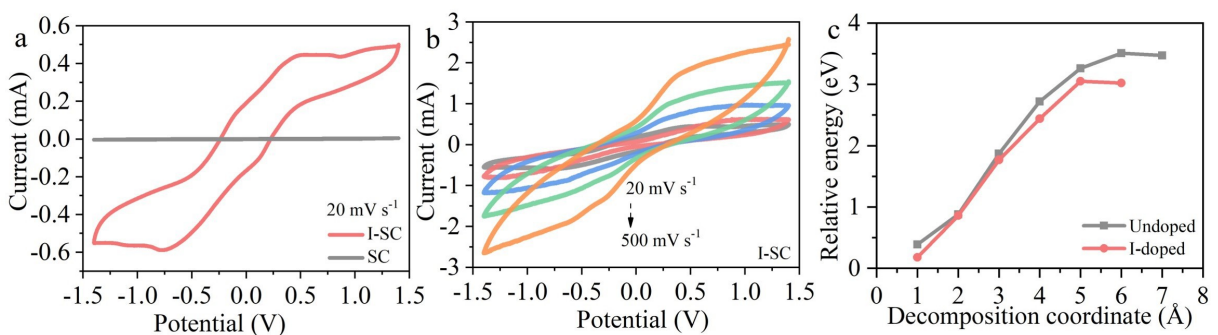


Figure 3. a) CV curve of symmetric cells employing I-SC and SC electrodes at 20 mV s⁻¹, b) cyclic voltammograms recorded at different scan rate of I-SC. c) Li₂S decomposition energy profiles on undoped and I-doped carbon.

have analyzed the Li₂S oxidation via studying the initial decomposition process of Li₂S, which contains the breaking of a Li–S bond and the Li ion moving away. Li₂S decomposition energy on I-doped carbon is much smaller than that on undoped carbon (Figure 3c), announcing an efficient catalytic effect to increase the speed of charging process.

Having proved that I-SC can adsorb polysulfide, we further introduce the iodine modified polypropylene separators (abbreviated as I-PP) as an effective method to obstruct the dissolution of LiPSs. First, we constructed a polydopamine (PDA) coating-PP, and then pretreated them in a HI solution. As shown in Figure S5, after PDA coating, the PP turns to black, and then turns to brown due to the adsorption of I⁻. In addition, the thermal shrinkages of PDA-PP did not change too

much. Furthermore, the electrolyte contact angle of PDA-PP and I-PP is smaller than that of PP, suggesting a good electrolyte wettability in PDA-PP and I-PP (Figure 4a–c). The morphology of PP, PDA-PP and I-PP was exhibited in Figure 4(d–f), all of them show a typical porous surface, and there are no obvious PDA particles on I-PP. Therefore, the PDA coating and immersion process have a trivial influence on the separator structure.

To confirm the formation of PDA and exist of I, the characterization of FTIR and XPS are conducted. As shown in Figure 4g, three peaks of 3439 cm⁻¹ (OH), 2916 cm⁻¹ (–CH₂, –CH₃), and 1609 cm⁻¹ (–NH) can be observed, indicating the formation of PDA in PDA-PP and I-PP. However, the C–I peaks of I-PP can hardly be distinguished due to their low

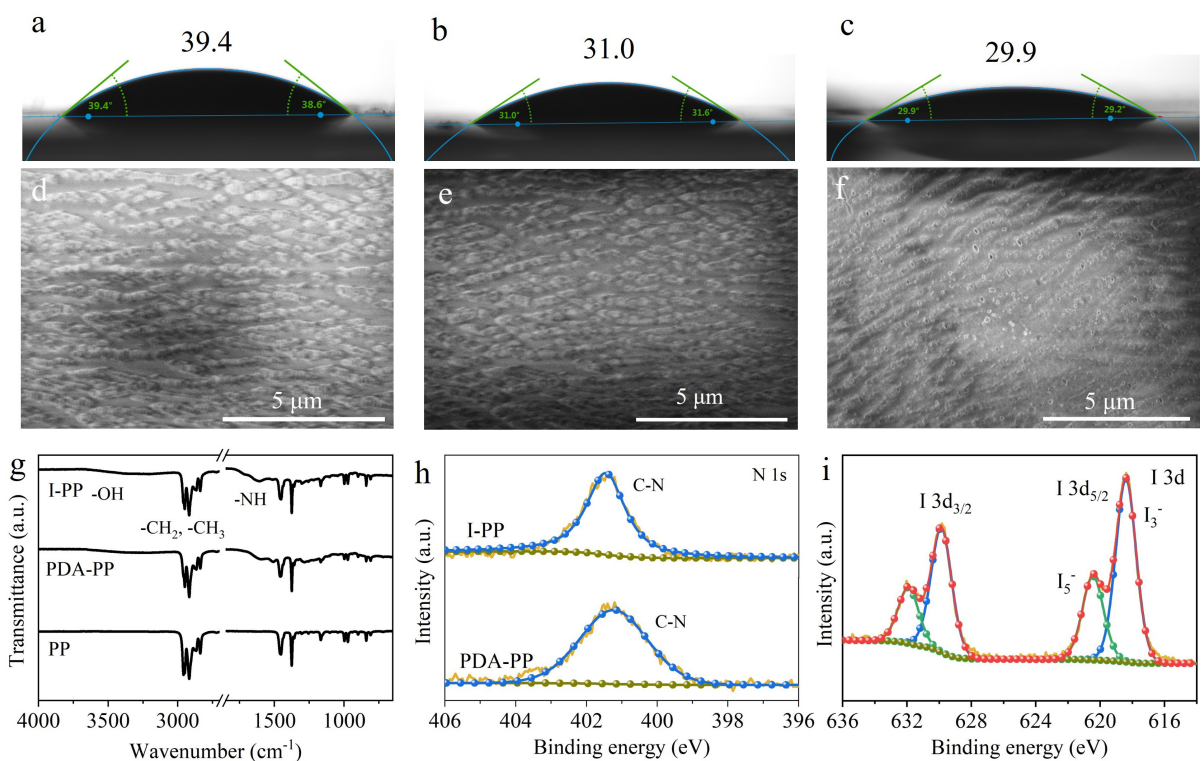
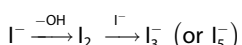


Figure 4. The contact angle of electrolyte on a) PP, b) PDA-PP, c) I-PP, SEM images of d) PP, e) PDA-PP, f) I-PP, g) FTIR, h) high-resolution XPS spectra of N 1s in PDA-PP and I-PP, i) I 3d in I-PP.

position. Therefore, XPS was carried out to further confirm the surface component of I-PP and the results are presented in Figures 4(h and i) and S6. The N 1s spectrum of PDA-PP and I-PP show a single peak at 400.1 eV (C—N), indicating the successful coating of PDA. The I 3d XPS spectrum in Figure 4i displays two typical I 3d peaks, which can be attributed to I 3d_{5/2} and I 3d_{3/2}. The I 3d_{5/2} spectrum of I-PP can be fitted as a sum of two peaks assigned to I₃⁻ (\approx 618.4 eV) and I₅⁻ (\approx 620.4 eV).^[28] The possible mechanism of polyiodide (I₃⁻ and I₅⁻) formation is attributed to the oxidation reaction of I⁻ in the presence of phenolic hydroxyl of poly-dopamine, and further react with I⁻ to form I₃⁻ and I₅⁻, which is depicted as the following equation:



Furthermore, to observe the dissolution of polysulfides across the separator, the visible H-type glass device was used to evaluate the infiltration effect of polysulfides in different separators. As performed in Figure S7, the polysulfides could easily crossover the PP separator within 2 h, and then the permeation becomes severe after 12 h. Surprisingly, the color of the blank DOL/DME (1:1) solution has no change even after 24 h, and thus the modified separator exhibits a good polysulfide inhibition behavior. As a result, we first successfully construct the polyiodide modified PP by covering it with dopamine used as a separator to further block the spread of polysulfide for Li-S batteries.

To verify the effect of I on the diffusion of Li⁺, the diffusion co-efficient of Li-ion was measured by CV and calculated according to the Randles-Sevcik equation:

$$I_p = 2.69 \times 10^5 n^{1.5} A D_{\text{Li}^+}^{0.5} \nu^{0.5} C_{\text{Li}^+}$$

where, I_p (A) is the peak current, n is the number of electrons transferred in the redox reaction ($n=2$ for Li-S batteries), A (cm⁻²) is the electrode area (1.13 cm⁻² here), ν is the scanning rate (V s⁻¹), $C(\text{Li}^+)$ (mol mL⁻¹) is the Li-ion concentration in the electrolyte, and $D(\text{Li}^+)$ is the lithium-ion diffusion coefficient (cm² s⁻¹).

Considering that there may be some LiPSs dissolved in the electrolyte, here the second cycle was selected for the test. The $D(\text{Li}^+)$ of I-SC/I-PP(1), I-SC/PP(2), SC/PDA-PP(3) and SC/PP(4) was measured by CV under different scanning rates from 0.1–0.4 mV s⁻¹ (Figure S8). For Li-S system, the two cathodic peaks at \sim 2.3 V and 2.0 V were marked as peak A and B, and the anodic peak at \sim 2.4 V was specified as peak C. The cathodic and anodic peaks (I_p) of these four electrodes showed a good linear relationship with $\nu^{0.5}$, indicating a diffusion-controlled process (Figure 5a). As shown in Figure 5(b), the $D(\text{Li}^+)$ of I-SC/I-PP and I-SC/PP are larger than that of SC/PDA-PP and SC/PP, demonstrating that I modified cathode and separator can both accelerate Li⁺ diffusion. In addition, when compared to SC/PP, the $D(\text{Li}^+)$ of SC/PDA-PP exhibits small-range increase, indicating that PDA-PP is affected less. The results of CV tests clearly verify that the Li-ion diffusion with I-SC and I-PP increased, further supporting that I-functional SC and PP can accelerate the migration of Li-ion.

Possessing thoroughly investigated the effectiveness of I-SC as sulfur support for Li-S batteries, we moved to study their rate and cycle properties. Figure 6(a) shows the electrochemical performance of I-SC/I-PP, I-SC/PP, SC/PDA-PP and SC/PP at various current densities. After I-doping, the I-SC exhibits average specific capacities of 1343, 1096, 926, 787, and 646 mAh g⁻¹ at 0.05, 0.1, 0.2, 0.5 and 1 C, respectively. Furthermore, assisting with I-PP, even under a large current density of 1 C, a notable capacity of 909 mAh g⁻¹ is still retained. As a contrast, SC electrodes rendered rather an inferior rate performance of 1065 to 325 mAh g⁻¹, when the current rate stepwise ramps from 0.05 to 1 C. Figure 6(b) present the cycling performances of I-SC/I-PP, I-SC/PP, SC/PDA-PP and SC/PP at 0.2 C. In comparison, the I-SC/I-PP exhibits a significantly improved cycling stability with a higher capacity retention of 956 mAh g⁻¹ than I-SC/PP and (900 mAh g⁻¹) after 300 cycles, which means that I-PP can further suppress the dissolution of LiPSs during cycling. Here, we noticed that the cycling stability (I-SC/I-PP > I-SC/PP > SC/PDA-PP > SC/PP) is quite different, and this phenomenon could be explained by stronger I-doping effect on both cathode and separator modification. SEM images of I-SC/S electrode before and after 100 cycles were shown in Figure S10. It can be seen that semi-

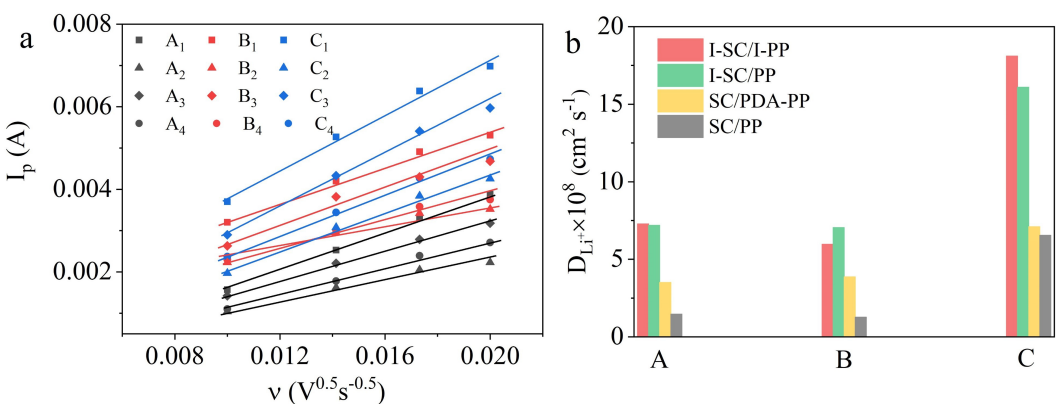


Figure 5. a) Peak currents (I_p) versus square root of scan rates ($\nu^{0.5}$), b) calculated the lithium-ion diffusion coefficients.

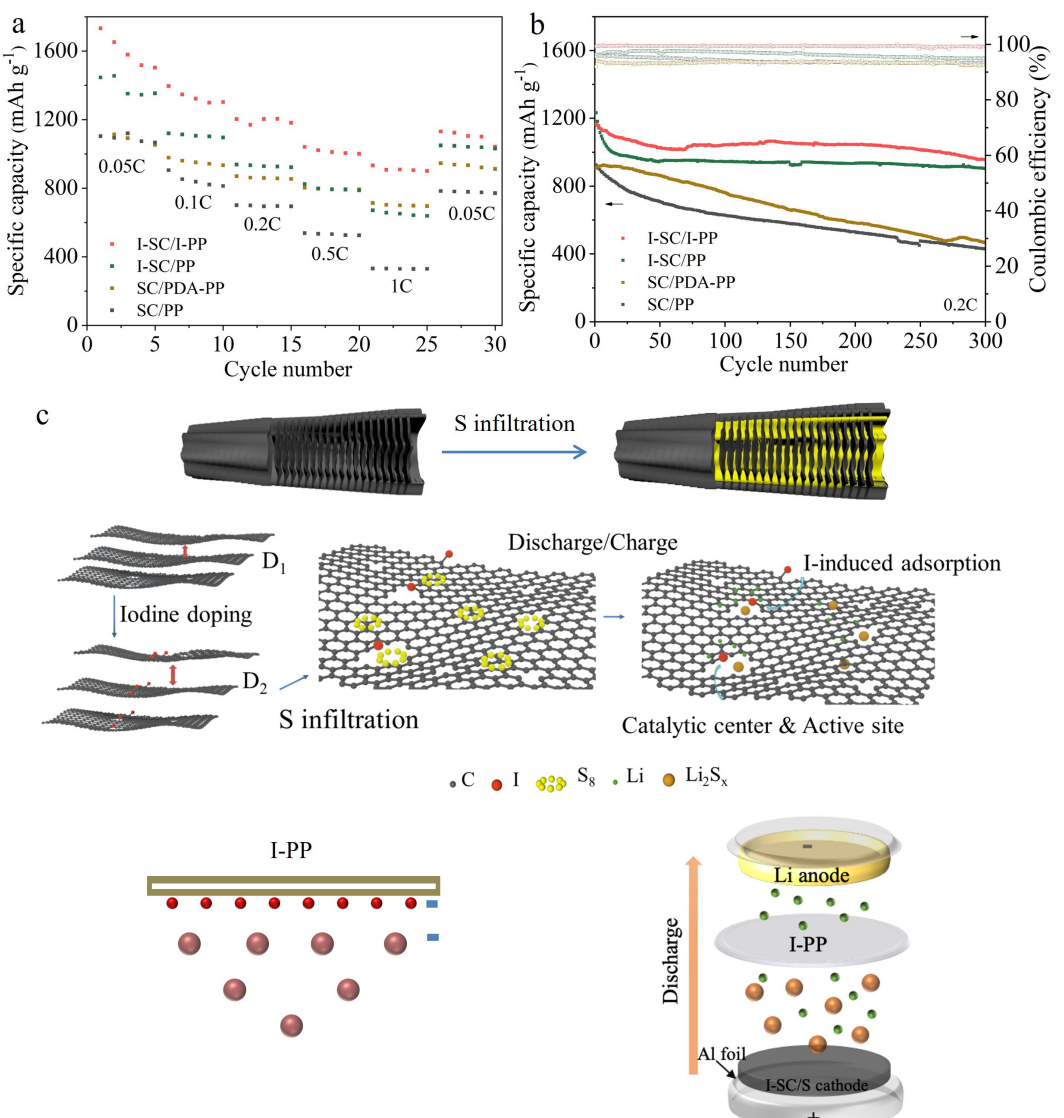


Figure 6. a) Rate performance, b) cycle performance of I-SC/I-PP, I-SC/PP, SC/PDA-PP and SC/PP, c) schematic illustration of the mechanism of I-doping for Li-S batteries.

hollow micro-rods structure of SC and I-SC remains undisturbed, which indicates that the structural integrity is the source of the excellent cycling stability.

In order to evaluate the positive effects of I dopants, we compared electrochemical performance of I-SC and I-SC/I-PP with several heteroatom doped carbon materials. And the results are exhibited in the Table S1. As shown in Figure 6(c), we designed two methods to improve electrochemical performance of this system. One is the cathode designing, the iodine doping plays three important functions. First of all, the enlarged interlayer distance (0.41 nm) is beneficial to boost the insertion/desertion of Li⁺. Second, the increased positive charge density on carbon plane, through surface charge transfer by I-doping, can effectively anchor the negative S_x²⁻ ($x=1, 2, 4, 6$), and inhibit the "shuttle effect". Third, the I-doping on carbon matrix can further facilitate the chemical adsorption ability and catalytic effect of polysulfide. The other

one is the modification of PP separator. The formation of triiodide (I₃⁻) and pentaiodide (I₅⁻) polyanions on separator can further block the polysulfide on the positive side from entering the negative side. The above results indicate that the dual-protection ways have potential in improving immobilization and conversion of polysulfides.

Conclusion

In summary, we have successfully designed and synthesized I-SC and I-PP. The introduction of iodine plays an important role in this system. First, I-doping increases the carbon interlayer distance. Next, I-doping can improve polysulfides adsorption and redox kinetics. Third, the decoration of separator with polyiodide anions (I₃⁻ and I₅⁻) can further inhibit the polysulfides into the anode side. To sum up, with the aid of iodine

functional PP, I-SC electrode displays superior rate performance (909 mAh g⁻¹ at 1 C) and good cycle stability (956 mAh g⁻¹ at 0.2 C for 300 cycles). We believe that this work may shed light on the development of iodine doping strategy for rechargeable batteries system.

Experimental Section

Synthesis I-SC and SC

In a typical synthesis procedure, iodine (300 mg) and 3,4,9,10-perylene tetracarboxylic dianhydride (PTCDA, 98%, Alfa Aesar) (400 mg) were dissolved in ethanol (40 mL). After stirring 6 h, 30 mL deionized water was added into the mixture. The mixed solution was stirred for another 12 h, and then vacuum filtrated and dried for further processing. Next, the obtained products were carbonized at 900 °C for 10 h under flowing argon atmosphere to obtain I-SC. Pure PTCDA was also carbonized directly to obtain SC sample.

Synthesis I-SC/S and SC/S

The I-SC/S was obtained by a melting-diffusion method. Briefly, the I-SC was mixed with sublimed sulfur in a ratio of 1:4. Then, the mixture was transferred into a sealed vessel filled with argon and heated at 155 °C for 12 h. For comparison, SC/S composites were also prepared using the same procedure.

Preparation I-grafted separators

The conventional method was carried out according to typical procedure.^[30] Dopamine hydrochloride (2 mg mL⁻¹) was dissolved in Tris-buffer solution (pH=8.5) by magnetic stirring. Then, PP membranes were pretreated by ethanol and then immersed in the Tris buffer solution for 12 h at room temperature. Subsequently, the samples were collected and washed by water and then dried in a vacuum at 60 °C. The PDA-coating samples were heated at 150 °C for 30 min. After that, the PDA-coated separators were immersed in HCl acid (55%) for 12 h and then washed and dried to obtain the I-grafted separators.

Preparation of Li₂S₆ in DOL and DME

A Li₂S₆ solution was prepared according to a reported method by dissolving stoichiometric amounts of sulfur powder and Li₂S into 1,2-dimethoxyethane and 1,3-dioxolane (DME/DOL, 1:1 in volume) at 60 °C overnight in an argon glovebox.^[31]

Materials characterization

The surface morphology of the as-prepared materials was examined by a scanning electron microscope (FESEM, Hitachi S-4800, Japan) and a transmission electron microscopy (TEM, FEI talos f200s). The sample crystallinity was investigated by a Bruker D8 Advance diffractometer using Cu K_α radiation ($\lambda = 1.5418 \text{ \AA}$). Thermogravimetric analysis (TGA) (HITACHI, TG/DTA7300) was carried out under a N₂ atmosphere at the heating rate of 10 °C min⁻¹. The optical contact angle measuring instrument (KRUSS DSA25, Germany) was used to measure the wettability of electrolytes. The Brunauer-Emmett-Teller (BET) measurement using N₂ absorption was performed on Micromeritics ASAP2460 analyzer. Raman spectroscopy was performed

on a WITec Alpha 300R with a 532 nm laser. Li₂S₆ solutions before and after contact with various absorbents were tested by UV-visible absorption spectrophotometry (SHIMADZU UV 2600 at a wavelength of 665 nm).

Electrochemical measurements

To prepare working cathodes, the obtained active material was blended with Ketjen Black and polyvinylidene difluoride (PVDF), at the mass ratio of 8:1:1, in N-methyl-2-pyrrolidone (NMP) to form a uniform slurry. Then, the slurry was cast onto an Al foil and dried at 60 °C for 12 h in a vacuum oven. Finally, the film was punched into disks with a diameter of 12 mm. The sulfur loading of each working electrode was 1.0–3.0 mg cm⁻² and the ratio of electrolyte to sulfur is 25 μL mg⁻¹ for each battery. Coin-type cells (2032) were assembled with lithium foils as the counter and reference electrodes and Celgard 2400 membrane as a separator. The liquid electrolyte was composed of 1 M lithium bis(trifluoromethanesulfonyl)imide (LiTFSI) dissolved in a mixture of 1,3-dioxolane (DOL) and dimethoxymethane (DME) (v: v, 1:1) with 1% LiNO₃ additive. Discharge/charge tests were carried out between 1.8 and 3.0 V (vs. Li/Li⁺) at various C rates (1 C = 1675 mA g⁻¹) with LAND-CT2001A battery testing system (Wuhan, China). Cyclic voltammetry (CV) measurements were performed on electrochemical workstation (CHI 600A, Shanghai Chenhua). In addition, impedance spectra were performed using electrochemical workstation (Zahner IM6ex) in the frequency range of 10 mHz to 100 kHz with the disturbance amplitude of 5 mV.

Computational method

Relaxation of structures and energy calculations of Graphene, polysulfides and their hybrid systems are carried out by using density functional theory as implemented in "Spanish Initiative for Electronic Simulations with Thousands of Atoms" (SIESTA) code. Initially individual systems such as Graphene and polysulfides are optimized separately and later hybrid structure is designed with these individual relaxed structures. A fragment of Graphene is taken with periodicity along y-axis and hydrogen terminated edge in x-direction. Sufficient vacuum along the direction of z-axis is provided. This void space will avoid artificial or spurious interaction among image systems. Relaxed polysulfide is placed on top of the optimized graphene surface and the whole system is again relaxed to find out the ground state of the hybrid system.

Split type double zeta basis with polarization is obtained to expand wavefunctions for achieving efficient and faster convergence. K-points grid (5×5×1) is utilized under Monkhorst pack method for calculations.^[32] A well-known Perdew-Burke-Ernzerhof (PBE) exchange correlation functional under Generalized Gradient approximation (GGA) has been adopted.^[33] Kinetic energy cut-off of 500 Ry is put throughout the optimization process.

Acknowledgements

Y. Zhang gratefully acknowledges the financial support from the National Natural Science Foundation of China (51572078, 51772086, 51872087 and 51971089), the National Science Foundation of Hunan Province (2018JJ2038, 2020JJ5021), the Major Science and Technology Program of Changsha (kq1804010), and the Outstanding Youth Project of Hunan Provincial Education Department (No.18B436). Y. Zhang acknowledges the China Scholarship Council for funding.

Conflict of Interest

The authors declare no conflict of interest.

Data Availability Statement

The data that support the findings of this study are available from the corresponding author upon reasonable request.

Keywords: functional separator · iodine doping · lithium sulfur batteries · soft carbon

- [1] a) F. Wu, J. Maier, Y. Yu, *Chem. Soc. Rev.* **2020**, *49*, 1569; b) J. Xie, Y. C. Lu, *Nat. Commun.* **2020**, *11*, 2499; c) D. L. Wood, M. Wood, J. Li, Z. Du, R. E. Ruther, K. A. Hays, N. Muralidharan, L. Geng, C. Mao, I. Belharouak, *Energy Storage Mater.* **2020**, *29*, 254.
- [2] a) R. Rajagopalan, Y. Tang, X. Ji, C. Jia, H. Wang, *Adv. Funct. Mater.* **2020**, *30*; b) L. Huang, J. Li, B. Liu, Y. Li, S. Shen, S. Deng, C. Lu, W. Zhang, Y. Xia, G. Pan, X. Wang, Q. Xiong, X. Xia, J. Tu, *Adv. Funct. Mater.* **2020**, *30*.
- [3] a) J. Guo, H. Pei, Y. Dou, S. Zhao, G. Shao, J. Liu, *Adv. Funct. Mater.* **2021**, *31*, 2010499; b) Y.-H. Liu, C.-Y. Wang, S.-L. Yang, F.-F. Cao, H. Ye, *J. Energy Chem.* **2022**, *66*, 429; c) Y. Yoshie, K. Hori, T. Mae, S. Noda, *Carbon* **2021**, *182*, 32; d) Z. Tong, L. Huang, J. Guo, Y. Gao, H. Zhang, Q. Jia, D. Luo, W. Lei, S. Zhang, *Carbon* **2022**, *187*, 451.
- [4] a) J. M. Soler, E. Artacho, J. D. Gale, A. Garcia, J. Junquera, P. Ordejón, D. Sanchez-Portal, *J. Phys. Condens. Matter* **2002**, *14*, 2745; b) Y. Hu, W. Chen, T. Lei, Y. Jiao, J. Huang, A. Hu, C. Gong, C. Yan, X. Wang, J. Xiong, *Adv. Energy Mater.* **2020**, *10*; c) A. Bhargav, J. He, A. Gupta, A. Manthiram, *Joule* **2020**, *4*, 285; d) X.-Y. Li, Q. Zhang, *J. Energy Chem.* **2022**, *65*, 302.
- [5] a) S. Huang, Z. Wang, Y. Von Lim, Y. Wang, Y. Li, D. Zhang, H. Y. Yang, *Adv. Energy Mater.* **2021**, *11*; b) Y. Liu, Z. Wei, B. Zhong, H. Wang, L. Xia, T. Zhang, X. Duan, D. Jia, Y. Zhou, X. Huang, *Energy Storage Mater.* **2021**, *35*, 12; c) Z. Zhao, Z. Yi, H. Li, R. Pathak, Z. Yang, X. Wang, Q. Qiao, *Nano Energy* **2021**, *81*; d) Z. Sun, S. Vijay, H. H. Heenen, A. Y. S. Eng, W. Tu, Y. Zhao, S. W. Koh, P. Gao, Z. W. Seh, K. Chan, H. Li, *Adv. Energy Mater.* **2020**, *10*; e) S. Zhou, S. Yang, X. Ding, Y. Lai, H. Nie, Y. Zhang, D. Chan, H. Duan, S. Huang, Z. Yang, *ACS Nano* **2020**, *14*, 7538; f) M. Zhang, W. Chen, L. Xue, Y. Jiao, T. Lei, J. Chu, J. Huang, C. Gong, C. Yan, Y. Yan, Y. Hu, X. Wang, J. Xiong, *Adv. Energy Mater.* **2019**, *10*; g) H. Mao, L. Liu, L. Shi, H. Wu, J. Lang, K. Wang, T. Zhu, Y. Gao, Z. Sun, J. Zhao, G. Gao, D. Zhang, W. Yan, S. Ding, *Sci. Bull.* **2020**, *65*, 803; h) H. Zhang, P. Zuo, J. Hua, Y. Ma, C. Du, X. Cheng, Y. Gao, G. Yin, *Electrochim. Acta* **2017**, *238*, 257; i) T. Boenke, P. Härtel, S. Dörfler, T. Abendroth, F. Schwotzer, H. Althues, S. Kaskel, *Batteries & Supercaps* **2021**, *4*, 989.
- [6] Q. Liu, X. Han, Q. Dou, P. Xiong, Y. Kang, S. W. Kang, B. K. Kim, H. S. Park, *Batteries & Supercaps* **2021**, *4*, 1843.
- [7] a) J. Liu, S. Xiao, L. Chang, L. Lai, R. Wu, Y. Xiang, X. Liu, J. Song Chen, *J. Energy Chem.* **2021**, *56*, 343; b) X. Lian, N. Xu, Y. Ma, F. Hu, H. Wei, H.-Y. Chen, Y. Wu, L. Li, D. Li, S. Peng, *Chem. Eng. J.* **2021**, *421*; c) C. S. Cheng, S. H. Chung, *Batteries & Supercaps* **2022**, *5*, e20210032.
- [8] a) Z. Shen, Z. Zhang, M. Li, Y. Yuan, Y. Zhao, S. Zhang, C. Zhong, J. Zhu, J. Lu, H. Zhang, *ACS Nano* **2020**, *14*, 6673–6682; b) J. Wu, J. Chen, Y. Huang, K. Feng, J. Deng, W. Huang, Y. Wu, J. Zhong, Y. Li, *Sci. Bull.* **2019**, *64*, 1875; c) E. Jing, L. Chen, S. Xu, W. Tian, D. Zhang, N. Wang, Z. Bai, X. Zhou, S. Liu, D. Duan, X. Qiu, *J. Energy Chem.* **2022**, *64*, 574.
- [9] a) S. D. Seo, S. Yu, S. Park, D. W. Kim, *Small* **2020**, *16*, e2004806; b) E. Troschke, C. Kensy, F. Haase, S. Dörfler, Y. Joseph, B. V. Lotsch, S. Kaskel, *Batteries & Supercaps* **2020**, *3*, 1069.
- [10] a) M. Chen, S. Zhao, S. Jiang, C. Huang, X. Wang, Z. Yang, K. Xiang, Y. Zhang, *ACS Sustainable Chem. Eng.* **2018**, *6*, 7545; b) D. Bosababu, R. Sampathkumar, G. Karkera, K. Ramesha, *Energy Fuels* **2021**, *35*, 8286; c) T. Z. Hou, X. Chen, H. J. Peng, J. Q. Huang, B. Q. Li, Q. Zhang, B. Li, *Small* **2016**, *12*, 3283.
- [11] a) C. Kensy, P. Härtel, J. Maschita, S. Dörfler, B. Schumm, T. Abendroth, H. Althues, B. V. Lotsch, S. Kaskel, *Carbon* **2020**, *161*, 190; b) H.-J. Peng, T.-Z. Hou, Q. Zhang, J.-Q. Huang, X.-B. Cheng, M.-Q. Guo, Z. Yuan, L.-Y. He, F. Wei, *Adv. Mater. Interfaces* **2014**, *1*; c) X. Wang, Z. Zhang, Y. Qu, Y.

Lai, J. Li, *J. Power Sources* **2014**, *256*, 361; d) L.-C. Yin, J. Liang, G.-M. Zhou, F. Li, R. Saito, H.-M. Cheng, *Nano Energy* **2016**, *25*, 203; e) H. Yuan, W. Zhang, J.-g. Wang, G. Zhou, Z. Zhuang, J. Luo, H. Huang, Y. Gan, C. Liang, Y. Xia, J. Zhang, X. Tao, *Energy Storage Mater.* **2018**, *10*, 1; f) S. Yuan, J. L. Bao, L. Wang, Y. Xia, D. G. Truhlar, Y. Wang, *Adv. Energy Mater.* **2016**, *6*; g) W. Yang, P. Wang, Z. Tu, L. Hou, L. Yan, B. Jiang, C. Zhang, G. Huang, F. Yang, Y. Li, *Carbon* **2022**, *187*, 338; h) J. H. Park, W. Y. Choi, J. Yang, D. Kim, H. Gim, J. W. Lee, *Carbon* **2021**, *172*, 624; i) Y. Liu, H. Guo, B. Zhang, G. Wen, R. Vajtai, L. Wu, P. M. Ajayan, L. Wang, *Batteries & Supercaps* **2020**, *3*, 1201.

- [12] a) J. Tan, D. Li, Y. Liu, P. Zhang, Z. Qu, Y. Yan, H. Hu, H. Cheng, J. Zhang, M. Dong, C. Wang, J. Fan, Z. Li, Z. Guo, M. Liu, *J. Mater. Chem. A* **2020**, *8*, 7980; b) J. Ren, L. Xia, Y. Zhou, Q. Zheng, J. Liao, D. Lin, *Carbon* **2018**, *140*, 30; c) W. Ai, W. Zhou, Z. Du, Y. Chen, Z. Sun, C. Wu, C. Zou, C. Li, W. Huang, T. Yu, *Energy Storage Mater.* **2017**, *6*, 112; d) J. Cai, C. Wu, Y. Zhu, K. Zhang, P. K. Shen, *J. Power Sources* **2017**, *341*, 165; e) C.-C. Chuang, Y.-Y. Hsieh, W.-C. Chang, H.-Y. Tuan, *Chem. Eng. J.* **2020**, *387*; f) B. Zheng, L. Yu, N. Li, J. Xi, *Electrochim. Acta* **2020**, *345*.
- [13] a) Q. Pang, J. Tang, H. Huang, X. Liang, C. Hart, K. C. Tam, L. F. Nazar, *Adv. Mater.* **2015**, *27*, 6021; b) S. Zhang, P. Zhang, R. Hou, B. Li, Y. Zhang, K. Liu, X. Zhang, G. Shao, *J. Energy Chem.* **2020**, *47*, 281; c) X. Yang, Z. Ran, F. Luo, Y. Li, P. Zhang, H. Mi, *Appl. Surf. Sci.* **2020**, *509*; d) P. H. Wadekar, A. Ghosh, R. V. Khose, D. A. Pethsangave, S. Mitra, S. Some, *Electrochim. Acta* **2020**, *344*; e) J. Li, J. Zhou, T. Wang, X. Chen, Y. Zhang, Q. Wan, J. Zhu, *Nanoscale* **2020**, *12*, 8991.
- [14] a) M. Chen, S. Jiang, C. Huang, X. Wang, S. Cai, K. Xiang, Y. Zhang, J. Xue, *ChemSusChem* **2017**, *10*, 1803; b) J. Ren, Y. Zhou, M. Guo, Q. Zheng, D. Lin, *Int. J. Hydrogen Energy* **2018**, *43*, 2002.
- [15] a) Y. Zhang, Y. Yang, C. Huang, H. Fan, D. Yuan, W.-B. Luo, A. Hu, Q. Tang, X. Chen, *Electrochim. Acta* **2021**, *394*; b) F. Yang, K. Huang, *Mater. Res. Express* **2021**, *8*; c) Z. Liu, X. Wang, A. Hu, Q. Tang, Y. Xu, X. Chen, *J. Cent. South Univ.* **2021**, *28*, 2345–2359.
- [16] a) Y. Li, W. Zhong, C. Yang, F. Zheng, Q. Pan, Y. Liu, G. Wang, X. Xiong, M. Liu, *Chem. Eng. J.* **2019**, *358*, 1147; b) Y. Liu, Y. X. Lu, Y. S. Xu, Q. S. Meng, J. C. Gao, Y. G. Sun, Y. S. Hu, B. B. Chang, C. T. Liu, A. M. Cao, *Adv. Mater.* **2020**, *32*, e2000505; c) X. Wang, K. Han, D. Qin, Q. Li, C. Wang, C. Niu, L. Mai, *Nanoscale* **2017**, *9*, 18216.
- [17] a) L. Fan, M. Li, X. Li, W. Xiao, Z. Chen, J. Lu, *Joule* **2019**, *3*, 361; b) D. Liu, C. Zhang, G. Zhou, W. Lv, G. Ling, L. Zhi, Q. H. Yang, *Adv. Sci.* **2018**, *5*, 1700270; c) X. Zhang, K. Chen, Z. Sun, G. Hu, R. Xiao, H.-M. Cheng, F. Li, *Energy Environ. Sci.* **2020**, *13*, 1076; d) C. Zhang, L. Cui, S. Abdolhosseini-zadeh, J. Heier, *InfoMat* **2020**, *2*, 613.
- [18] a) Z. Wei, Y. Ren, J. Sokolowski, X. Zhu, G. Wu, *InfoMat* **2020**, *2*, 483; b) M. Chen, X. Zhao, Y. Li, P. Zeng, H. Liu, H. Yu, M. Wu, Z. Li, D. Shao, C. Miao, G. Chen, H. Shu, Y. Pei, X. Wang, *Chem. Eng. J.* **2020**, *385*; c) C. Qi, L. Xu, J. Wang, H. Li, C. Zhao, L. Wang, T. Liu, *ACS Sustainable Chem. Eng.* **2020**, *8*, 12968; d) X. Song, S. Wang, G. Chen, T. Gao, Y. Bao, L.-X. Ding, H. Wang, *Chem. Eng. J.* **2018**, *333*, 564; e) Z. Zhang, A. H. Shao, D. G. Xiong, J. Yu, N. Koratkar, Z. Y. Yang, *ACS Appl. Mater. Interfaces* **2020**, *12*, 19572; f) X. Yu, H. Wu, J. H. Koo, A. Manthiram, *Adv. Energy Mater.* **2019**, *10*; g) Y. Chen, P. Xu, Q. Liu, D. Yuan, X. Long, S. Zhu, *Carbon* **2022**, *187*, 187.
- [19] Y. He, Y. Qiao, Z. Chang, X. Cao, M. Jia, P. He, H. Zhou, *Angew. Chem. Int. Ed. Engl.* **2019**, *58*, 11774.
- [20] X. Yao, Y. Ke, W. Ren, X. Wang, F. Xiong, W. Yang, M. Qin, Q. Li, L. Mai, *Adv. Energy Mater.* **2018**, *9*.
- [21] H. L. Wu, L. A. Huff, A. A. Gewirth, *ACS Appl. Mater. Interfaces* **2015**, *7*, 1709.
- [22] F. Xu, S. Yang, X. Chen, Q. Liu, H. Li, H. Wang, B. Wei, D. Jiang, *Chem. Sci.* **2019**, *10*, 6001.
- [23] S. Ma, P. Zuo, H. Zhang, Z. Yu, C. Cui, M. He, G. Yin, *Chem. Commun. (Camb.)* **2019**, *55*, 5267.
- [24] a) H. Liu, P. Zeng, Y. Li, H. Yu, M. Chen, S. Jamil, C. Miao, G. Chen, Q.-C. Liu, Z. Luo, X. Wang, *ACS Sustainable Chem. Eng.* **2020**, *8*, 16659; b) P. Xiong, X. Han, X. Zhao, P. Bai, Y. Liu, J. Sun, Y. Xu, *ACS Nano* **2019**, *13*, 2536–2543.
- [25] Q. He, A. T. S. Freiberg, M. U. M. Patel, S. Qian, H. A. Gasteiger, *J. Electrochem. Soc.* **2020**, *167*.
- [26] a) J. Wu, Q. Ma, C. Lian, Y. Yuan, D. Long, *Chem. Eng. J.* **2019**, *370*, 556; b) X. Liang, C. Y. Kwok, F. Lodi-Marzano, Q. Pang, M. Cuisinier, H. Huang, C. J. Hart, D. Houtarde, K. Kaup, H. Sommer, T. Brezesinski, J. Janek, L. F. Nazar, *Adv. Energy Mater.* **2016**, *6*; c) X. Liang, C. Hart, Q. Pang, A. Garsuch, T. Weiss, L. F. Nazar, *Nat. Commun.* **2015**, *6*, 5682; d) M. Li, X. Zhou, X. Liu, L. Chen, D. Zhang, S. Xu, D. Duan, Q. Yuan, L. Ling, S. Liu, *Batteries & Supercaps* **2021**, *5*.

- [27] E. Olsson, G. Chai, M. Dove, Q. Cai, *Nanoscale* **2019**, *11*, 5274.
- [28] a) C. Wang, L. Sun, K. Li, Z. Wu, F. Zhang, L. Wang, *ACS Appl. Mater. Interfaces* **2020**, *12*, 43560; b) Z. Li, Z. Xiao, P. Li, X. Meng, R. Wang, *Small* **2020**, *16*, e1906114.
- [29] W. Zhu, Z. Zhang, J. Wei, Y. Jing, W. Guo, Z. Xie, D. Qu, D. Liu, H. Tang, J. Li, *J. Membr. Sci.* **2020**, 597.
- [30] a) M. Wu, J. Yuan, H. Wu, Y. Su, H. Yang, X. You, R. Zhang, X. He, N. A. Khan, R. Kasher, Z. Jiang, *J. Membr. Sci.* **2019**, *576*, 131; b) N. Liu, M. Zhang, W. Zhang, Y. Cao, Y. Chen, X. Lin, L. Xu, C. Li, L. Feng, Y. Wei, *J. Mater. Chem. A* **2015**, *3*, 20113.
- [31] P. Li, H. Lv, Z. Li, X. Meng, Z. Lin, R. Wang, X. Li, *Adv. Mater.* **2021**, *33*, 2007803.
- [32] H. J. Monkhorst, J. D. Pack, *Phys. Rev. B* **1976**, *13*, 5188.
- [33] J. P. Perdew, K. Burke, M. Ernzerhof, *Phys. Rev. Lett.* **1996**, *77*, 3865.

Manuscript received: March 16, 2022
Revised manuscript received: April 13, 2022
Accepted manuscript online: April 19, 2022
Version of record online: June 2, 2022
